Fractionalization of Majorana-Ising-type quasiparticle excitations

J. E. Sanches [1,*] L. T. Lustosa,[1] L. S. Ricco [2] I. A. Shelykh,[2,3] M. de Souza [4] M. S. Figueira,[5] and A. C. Seridonio [1,†]

[1]*São Paulo State University (Unesp), School of Engineering,*
Department of Physics and Chemistry, 15385-000, Ilha Solteira-SP, Brazil
[2]*Science Institute, University of Iceland, Dunhagi-3, IS-107, Reykjavik, Iceland*
[3]*Abrikosov Center for Theoretical Physics, MIPT, Dolgoprudnyi, Moscow Region 141701, Russia*
[4]*São Paulo State University (Unesp), IGCE, Department of Physics, 13506-970, Rio Claro-SP, Brazil*
[5]*Instituto de Física, Universidade Federal Fluminense, 24210-340, Niterói, Rio de Janeiro, Brazil*

We theoretically investigate the spectral properties of a quantum impurity (QI) hosting the here proposed Majorana-Ising-type quasiparticle excitation. It arises from the coupling between a finite topological superconductor (TSC) based on a chain of magnetic adatoms–superconducting hybrid system and an integer large spin S flanking the QI. It is noteworthy that the spin S couples to the QI via the Ising-type exchange interaction. As the Majorana zero modes (MZMs) at the edges of the TSC chain are overlapped, we counterintuitively find a regime wherein the Ising term modulates the localization of a fractionalized and resonant MZM at the QI site. Interestingly enough, the fermionic nature of this state is revealed as purely of the electron tunneling type and, most astonishingly, it has the Andreev conductance completely null in its birth. Therefore, we find that a resonant edge state appears as a zero mode and discuss it in terms of a *poor man's Majorana* [Dvir *et al.*, Nature **614**, 445 (2023)].

I. INTRODUCTION

Majorana fermions are peculiar particles equal to their own antiparticles described by real solutions of the Dirac equation [1]. In condensed matter physics, such fermions rise as quasiparticle excitations usually called Majorana zero modes (MZMs), which are found attached to the boundaries of topological superconductors (TSCs) [2–31]. Astonishingly, since the theoretical Kitaev seminal proposal of *p-wave* superconductivity [32], MZMs are notably coveted due to their attribution as building blocks for the highly pursued fault-tolerant topological quantum computing. Thereafter, in the last few years, such excitations have received astounding focus from both communities working with quantum science and technology.

Interestingly enough, theoretical predictions point out that the fractional zero-bias peak (ZBP) in transport evaluations through quantum dots, which is given by the conductance $\mathcal{G}_{\text{total}}(0) = \frac{e^2}{2h}$ [2–4], could have its origin from both the system topological nontrivial regime, where two MZMs emerge spatially far apart at the edges of a TSC [3,4], as well as in the corresponding trivial, which could exhibit, for instance, Andreev bound states (ABSs) [33,34]. In this regard, we highlight Ref. [35], which, by treating the TSC within the theoretical framework of the Oreg-Lutchyn Hamiltonian [9], allows a detailed and systematic analysis on the for-

mation of MZMs versus ABSs issue. In parallel, effective models [3,33,36], despite their simplifications, are used to capture, with quite good accuracy, the corresponding low-energy physics encoded by models such as that in Ref. [9] and the Kitaev Hamiltonian [32].

Back to the issue of the topological nontrivial regime, not less important, once an ordinary fermion can be decomposed into two MZMs, is the amplitude $1/2$ in $\mathcal{G}_{\text{total}}(0)$, the hallmark of the fractionalization of the quantum of conductance $\frac{e^2}{h}$, thus giving rise to the concept of fractionalized electronic zero-frequency spectral weight, which indeed reveals the MZM half-fermionic nature [4]. This aforementioned fingerprint is expected to show up in engineered platforms that combine conventional *s-wave* superconductivity and spin-texture [see Refs. [37–39] and Fig. 1(a)]. As aftermath, the *p-wave* superconductivity becomes feasible, thus allowing the experimental realization of the spinless Kitaev wire, which is indeed, a TSC in 1D [7,25,27,32,40–43]. For such an accomplishment, we highlight two practical recipes based on the Oreg-Lutchyn proposal [9], which have the following ingredients: (i) a semiconducting nanowire, with strong spin-orbit coupling (SOC) and under a magnetic field, should be deposited on top of an *s-wave* superconductor [6,25,29–31,40,41] or (ii) a linear chain of magnetic adatoms with exchange interactions should be hosted by an *s-wave* superconductor with strong SOC [12,13,18,37–39,44–49]. In both situations, the *s-wave* superconductors with singlet Cooper pairing lead to the so-called superconducting proximity effect, which is pivotal to carry forward the superconducting (SC) character into such manufactured Kitaev wires. Thus, the Zeeman field from the previous recipes (i) and (ii), together with the magnified

---

*Corresponding author: jose.sanches@unesp.br
†Corresponding author: antonio.seridonio@unesp.br

155144-1
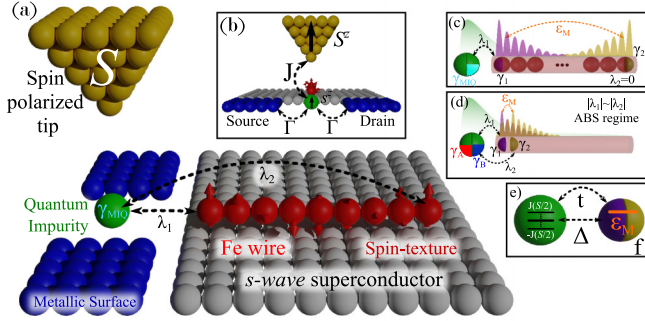
FIG. 1. (a) Proposed device expected to show a Majorana-Ising-type quasiparticle (MIQ) excitation γ_{MIQ} localized at the quantum impurity (QI) site. The γ_{MIQ} leads to a zero-bias conductance peak $\mathcal{G}_{\mathrm{MIQ}}(0) = \frac{e^2}{4h}$ due to the QI placed between source and drain leads, but the total conductance is still $\mathcal{G}_{\mathrm{total}}(0) = \frac{e^2}{2h}$. This occurs once a genuine electron tunneling (ET) process is present and there is a complete lack of local Andreev (LAR) reflection. It can be performed by considering the QI simultaneously coupled to a spin-polarized tip with an integer large spin S via an Ising-type exchange interaction J and with the hopping terms $\lambda_{1(2)}$ (being $\lambda_2 = 0$ for this case) to a helical spin-texture chain hosted by an s-wave superconductor. (b) Side view of (a) wherein the QI-lead coupling Γ and Ising-type exchange interaction J for the spin-polarized tip and QI appear highlighted. (c) Pictorial scheme of (b), which effectively consists of a topological superconductor (TSC), where ε_M represents the overlap between the Majorana zero modes (MZMs) γ_1 and γ_2 at edges, while the QI shows the MIQ γ_{MIQ}. The spatial distributions of the wave functions for the MZMs and QI are also illustrated. The factor $\frac{1}{4}$ in $\mathcal{G}_{\mathrm{MIQ}}$ has correspondence to the $\frac{1}{4}$ from the volume for the sphere depicted to represent the quasiparticle γ_{MIQ}, in contrast to the ratio $\frac{1}{2}$ for the typical volume of the MZMs γ_1 and γ_2. (d) Andreev bound state (ABS) regime, obtained from the effective model with $|\lambda_1| \sim |\lambda_2|$ [33]. (e) These MZMs mimic a delocalized fermionic site f, wherein ε_M plays the role of its energy level, while the QI has $2S + 1$ levels ranging from $-J(S/2)$ to $+J(S/2)$. In this scenario, such quantum dots constitute a Kitaev dimer, i.e., with hopping t and pairing $\triangle$ of the p-wave Cooper pair split into the QI and f orbitals.

FIG. 2. (a) Total differential conductance $\mathcal{G}_{\mathrm{total}}$ [Eq. (5)] versus the source-drain bias-voltage eV in units of the QI-lead coupling Γ with isolated MZMs γ_1 and $\gamma_2(\varepsilon_M = 0)$ in the absence of a spin-polarized tip ($S = 0$). As aftermath, a zero-bias peak (ZBP) emerges with amplitude $\mathcal{G}_{\mathrm{total}}(0) = \frac{e^2}{2h}$ and characterizes the leaking of the MZM γ_1 from the TSC wire edge [Fig. 1(c)] into the QI as γ_A (Fig. 3(a)I and Refs. [3,4]). (b) The ZBP conductance can be split into finite contributions from the electron tunneling (ET) and local Andreev reflection (LAR) processes [Eq. (5)], namely, $\mathcal{G}_{\mathrm{ET}}(0)$ and $\mathcal{G}_{\mathrm{LAR}}(0)$, respectively. This corresponds to the ideal case of an infinite TSC wire, wherein these processes compete on equal footing. (c) In the presence of a tip with $S = 3$ and exchange coupling at the sweet spot $J = J_{\mathrm{h}} = 1.335\Gamma$ [Fig. 3(b)I] for a finite wire ($\varepsilon_M = 1\Gamma$), the amplitude $\mathcal{G}_{\mathrm{total}}(0) = \frac{e^2}{2h}$ is still observed and denotes the existence of a MIQ γ_{MIQ} within the QI, but with related differential conductance $\mathcal{G}_{\mathrm{MIQ}}(0) = \frac{e^2}{4h}$ [Fig. 3(c) and Eqs. (23) and (24)]. (d) In the regime of (c), $\mathcal{G}_{\mathrm{LAR}}(0)$ is completely quenched and solely the term $\mathcal{G}_{\mathrm{ET}}(0)$ contributes to the ZBP.

SOC from such quantum materials, establish a synergy that stabilizes the system spin-texture and, consequently, the triplet Cooper pairing for the p-wave superconductivity as well.

Particularly in the topological nontrivial regime of such setups, these Majorana quasiparticle excitations emerge ideally, i.e., as MZMs decoupled from each other and localized on the boundaries of the TSC. Due to this decoupling from their environment, MZMs are regarded robust against perturbations, once they are topologically protected by the SC gap. Thus, MZMs become promising candidates for a quantum computing free of the decoherence phenomenon [50,51]. However, perfectly far apart, MZMs are hypothetical objects since they are reliable solely in infinite-size systems and in real experiments, the quantum wires are finite. As a result, these end MZMs within a finite length overlap with each other and, inevitably, a fermionic mode with a finite energy emerges instead.

To overcome the aforementioned challenge, in this paper, we find as a route the fractionalization of ordinary MZMs, in particular, those found at a quantum impurity (QI) site coupled

to one edge of a finite TSC in 1D. To this end, we should take into account the Ising exchange interaction between an integer large spin and such a QI. This setup corresponds to Figs. 1(a) and 1(b), and it contains the ordinary MZMs γ_1 and γ_2 placed at the edges of a short TSC wire. To better understand our findings, we propose to view the MZMs as sketched in Fig. 1(c), where these objects appear symbolized by calottes (half spheres). We clarify that the employment of such a pictorial representation for the MZMs aims to explain diagrammatically the electron fractionalization into them, as well as the MZM fractionalization itself here observed. These calottes belong to a delocalized sphere cut in half, with each part placed at the TSC edges. This cartoon is very useful and it has the purpose of emulating the nonlocal nature of the fermionic state composed by these MZMs, which are found spatially far apart. To the best of our knowledge, the Majorana zero-frequency spectral weight, in particular, for a QI coupled to an infinite TSC, is given by the unity when the leaking of the MZM γ_1 into a quantum dot occurs [4]. This unity corresponds to a calotte, which is a half-electron state that contributes to the conductance $\mathcal{G}_{\mathrm{MZM}}(0) = \frac{e^2}{2h}$, as expected [3,4]. Particularly for a finite TSC, we define as the system sweet spot [see Fig. 3(b)I] a special configuration, in which a peculiar Ising exchange interaction allows us to observe a fractionalized MZM quasiparticle excitation γ_{MIQ} at
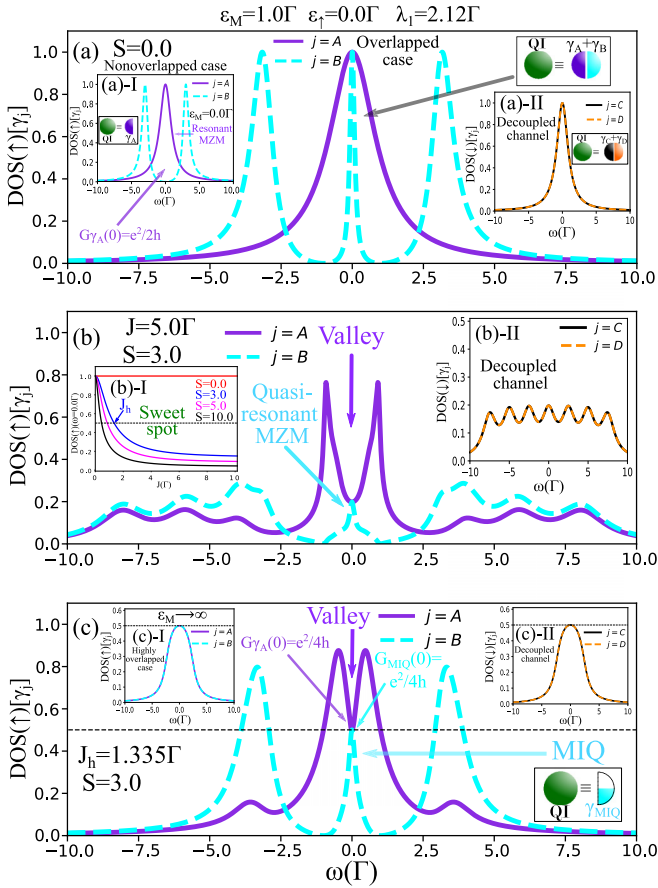
FIG. 3. (a) The central panel shows the frequency dependence of the normalized densities of states (DOS) for the MZMs γ_A and γ_B [Eq. (21)] for the spin-up channel within the QI by assuming the spin-polarized tip absent and the MZMs γ_1 and γ_2 overlapped ($\varepsilon_M = 1\Gamma$) in the TSC. In each DOS, we find a resonant MZM, which corresponds to a half-fermionic state of the QI depicted as the green sphere in the upper-right inset. This sphere has inner MZMs represented by calottes to denote the half-fermion nature of the MZM. In the nonoverlapped situation, only the calotte γ_A prevails [inset (a)I]. It leads to $\mathcal{G}_{\text{total}}(0) = \mathcal{G}_{\gamma_A}(0) = \frac{e^2}{2h}$ in Fig. 2(a) [Eqs. (23) and (24)]. For the spin-down channel, which is decoupled from the TSC, the MZMs γ_C and γ_D within the QI stay paired permanently [inset (a)II]. (b) In the presence of $S = 3$ and $J = 5\Gamma$ for $\varepsilon_M = 1\Gamma$, the DOS for γ_A changes drastically, exhibiting a valley at $\omega = 0$ instead of a peak, while for γ_B the zero mode is not well-defined. To restore the ZBP $\mathcal{G}_{\text{total}}(0) = \frac{e^2}{2h}$, we should choose the right J for a given S, i.e., the sweet spot $J = J_h$ [panel (b)I for the QI DOS of Eq. (22), imposing DOS($\uparrow$)(0) = 1/2]. In the spin-down channel, the γ_C and γ_D DOS are degenerate with a $2S + 1$ multilevel structure [panel (b)II]. (c) The choice $J = J_h = 1.335\Gamma$ for $S = 3$ completely defines the valley and peak for the DOS γ_A and γ_B, respectively, where in the latter we introduce $\gamma_B \equiv \gamma_{\text{MIQ}}$ as the Majorana-Ising quasiparticle, once the peak clearly represents the unique MZM isolated in the system. It is characterized by a ZBP given by $\mathcal{G}_{\text{MIQ}}(0) = \frac{e^2}{4h}$ pictorially illustrated by the half calotte in the lower-right inset for the green sphere representing the QI fermionic state. However, $\mathcal{G}_{\text{total}}(0) = \mathcal{G}_{\gamma_A}(0) + \mathcal{G}_{\text{MIQ}}(0) = \frac{e^2}{2h}$.

the QI, namely, what we call a Majorana-Ising-type quasiparticle (MIQ) excitation [Figs. 1(a) and 1(c)]. This quasiparticle excitation can be viewed as the half calotte within the cartoon

representation of the QI state [see also Fig. 1(c)]. Such a ratio symbolizes an MZM-type excitation in the presence of finite TSCs, in which, technically speaking, it is identified by a Majorana zero-frequency spectral weight equals half. Equivalently, the same amount corresponds to $\frac{1}{4}$ of the entire QI electronic state. In contrast, it leads to $\mathcal{G}_{\text{MIQ}}(0) = \frac{e^2}{4h}$ as it should. Interestingly enough, solely in one of the Majorana density of states (DOS) of the QI, the MIQ becomes evident as a resonant mode localized at $\omega = 0$. Counterintuitively, the other Majorana DOS of the QI, instead of exhibiting a resonant state, reveals a Majorana zero-frequency spectral weight with a valley, but presenting the same magnitude of the resonant Majorana fermion. In this manner, we can safely state that this MZM-type quasiparticle excitation, which for simplicity, we just call MIQ from now on, is then found at the QI. In this situation, we demonstrate that the emergence of such a quasiparticle excitation yields a zero-bias local Andreev conductance entirely null, with only normal electronic contribution to the total conductance.

II. THE MODEL

The effective system Hamiltonian that corresponds to the proposed setup presented in Fig. 1(a) can be expressed as

$$\mathcal{H} = \sum_{\alpha k \sigma} \varepsilon_{\alpha k} c^\dagger_{\alpha k \sigma} c_{\alpha k \sigma} + \sum_\sigma \varepsilon_\sigma d^\dagger_\sigma d_\sigma + i \varepsilon_M \gamma_1 \gamma_2$$

$$+ \left(\frac{\Gamma}{2\pi\rho_0}\right)^{1/2} \sum_{\alpha k \sigma} (c^\dagger_{\alpha k \sigma} d_\sigma + \text{H.c.}) + J s^z S^z$$

$$+ \lambda_1 (d_\uparrow - d^\dagger_\uparrow)\gamma_1 + \lambda_2 (d_\uparrow + d^\dagger_\uparrow)\gamma_2, \quad (1)$$

where the operator $c^\dagger_{\alpha k \sigma}$ ($c_{\alpha k \sigma}$) describes the creation (annihilation) of an electron with momentum k, spin-z $\sigma = \pm 1$, energy $\varepsilon_{\alpha k} = \varepsilon_k - \mu_\alpha$ for the metallic lead $\alpha = $ [source, drain] in terms of the single-particle energy ε_k and chemical potential μ_α, while $d^\dagger_\sigma$ (d_σ) stands for the electrons at the QI site in which ε_σ represents their energy levels per spin. To connect the QI to the metallic leads and a large spin S as well, we should consider the QI-lead coupling $\Gamma = 2\pi v^2 \rho_0$, which is determined by the QI-lead hopping term v and lead DOS ρ_0, in parallel to the Ising-type exchange interaction J [Fig. 1(b)]. This Ising Hamiltonian involves the components s^z and S^z of the QI ($s = 1/2$) and S, respectively, wherein the latter could be well-represented, within an experimental framework, by a spin-polarized tip [Ref. [52] and Figs. 1(a) and 1(b)]. The emergence of MZMs at the TSC wire edges are accounted for, γ_1 and γ_2, with ε_M as the overlap parameter. Finally, λ_1 and λ_2 couple the spin-up channel of the QI to γ_1 and γ_2, respectively [Figs. 1(a) and 1(c)]. Additionally, for the sake of simplicity, we consider that the spin-down degree is decoupled from the TSC and obeys the single impurity Anderson model [53]. Thus, we assume that the spin component of the QI that couples to the Kitaev wire is $\sigma = +1$, which is, as can be viewed in Fig. 1(a), the same spin direction assumed for the edges of the magnetic chain of adatoms. This means that the spin flips of the QI electron injected into the TSC and vice versa are prevented. Therefore, the spin-up degree of the QI is unique to perceive the TSC. Different spin textures on the TSC edge where γ_1 is found [54], which would allow

the mixing of the spin degrees of freedom, will be addressed elsewhere and do not belong to the current analysis. Additionally, as we assume the intrinsic Zeeman splitting $\varepsilon_\downarrow - \varepsilon_\uparrow = V_Z$ of the magnetic chain as the largest energy scale, the spin down has no influence in the phenomenon here reported, once the corresponding electronic occupation is empty. However, even with the present assumption, we are free to demonstrate that both these spin components become influenced by S and the TSC that mimics an effective quantum dot tunnel and Andreev-coupled to the QI (Fig. 1(e), [55,56]).

To this end, note that the Majorana and Ising terms of Eq. (1) should be conveniently rewritten to access the system's underlying physics: (i) the Ising term turns straightforwardly into

$$J s^z S^z = \frac{J}{2} \sum_{m\sigma} \sigma m d_\sigma^\dagger d_\sigma |m\rangle\langle m| \quad (2)$$

due to the standard expansions $s^z = \frac{1}{2}\sum_\sigma \sigma d_\sigma^\dagger d_\sigma$ and $S^z = \sum_m m|m\rangle\langle m|$, with $m = [-S, -S+1, ..., S-1, S]$ for the QI and large spin, respectively. This means that each spin channel in the QI acquires a multilevel structure split into $2S+1$ energies ranging from $-J(S/2)$ to $+J(S/2)$. As a matter of fact, the TSC alters this feature quite a bit for the channel $\sigma = +1$; and (ii) it is imperative to evoke that the MZMs are made by the electron ($f^\dagger$) and hole (f) of a regular Dirac fermion delocalized over the TSC edges, which lead to $\gamma_1 = \frac{1}{\sqrt{2}}(f^\dagger + f)$ and $\gamma_2 = \frac{i}{\sqrt{2}}(f^\dagger - f)$. In this picture, ε_M plays the role of the energy level related to the electronic occupation $f^\dagger f$ and the QI is indeed hybridized with f, as mentioned earlier, via the hopping t and the superconducting pairing Δ. In summary, by considering the parametrization $\lambda_1 = (t+\Delta)/\sqrt{2}$ and $\lambda_2 = i(\Delta - t)/\sqrt{2}$ [Fig. 1(a)], we simply find the Kitaev dimer composed by $d_\uparrow$ and f orbital sites [55,56]:

$$i\varepsilon_M \gamma_1 \gamma_2 + \varepsilon_\uparrow d_\uparrow^\dagger d_\uparrow + \lambda_1(d_\uparrow - d_\uparrow^\dagger)\gamma_1 + \lambda_2(d_\uparrow + d_\uparrow^\dagger)\gamma_2$$
$$= \varepsilon_M\left(f^\dagger f - \frac{1}{2}\right) + \varepsilon_\uparrow d_\uparrow^\dagger d_\uparrow + (t d_\uparrow f^\dagger + \Delta d_\uparrow f + \text{H.c.}). \quad (3)$$

Similarly, the spin-up channel of the QI can be also decomposed in MZMs [4], which we label by γ_A and γ_B, i.e.,

$$d_\uparrow = \frac{1}{\sqrt{2}}(\gamma_A + i\gamma_B). \quad (4)$$

Based on Eq. (4), one can compute the Majorana zero-frequency spectral weights for γ_A and γ_B, respectively. These quantities reveal that in the *poor man's Majorana* regime ($J = 0$, $\Delta = t$ and $\varepsilon_M = \varepsilon_\uparrow = 0$) [55,56] for the Kitaev dimer, that at the QI site, one spectral weight shows a unitary amplitude for a resonant zero mode, while the other is completely null at zero energy. It means that an isolated MZM is found at the QI. Analogously, such a feature is also observed in f [4,32]. This results, according to Eq. (3) given by $i\sqrt{2}\lambda_1\gamma_B\gamma_1$, in two isolated MZMs spatially placed at $d_\uparrow$ and f orbital sites, namely, γ_A and γ_2, respectively. Although f is already nonlocal and split over the TSC edges, it should be understood as an orbital site in the framework of the Kitaev dimer, thus γ_2, within such a context, is placed there. For the trivial case

($\varepsilon_M \neq 0$), the two spectral weights for γ_A and γ_B attain to unity, and then two resonant zero-modes emerge at the QI site. Thus, Eq. (4) is extremely clarifying, once it points out the possibility of having within the QI, in the presence of ε_M and J, the isolation of the here proposed MIQ. Additionally, as one can see, the spin-down channel always shows the trivial case due to its decoupling from the TSC. For completeness, we label the MZMs for $d_\downarrow$ by γ_C and γ_D. To conclude, we are aware that the QI could also be coupled to the *s-wave* platform of Fig. 1(a) as in Ref. [49] by the term $\mathcal{H}_{s-QI} \sim -\Gamma_s(d_\uparrow^\dagger d_\downarrow^\dagger + \text{H.c.})$ [36,49] in the limit $\Delta_{SC} \to \infty$ (infinite superconducting gap standard approximation), where Γ_s is the s-wave-QI coupling. Nevertheless, differently, we do not consider the on-top geometry of Ref. [49] and assumes intrinsic Zeeman splitting $\varepsilon_\downarrow - \varepsilon_\uparrow = V_Z$ of the magnetic chain extremely high to rid off the spin-down component. As a result, we expect that both features suppress $\mathcal{H}_{s-QI}$ and leave the exploration to elsewhere when V_Z is not found magnified.

III. QUANTUM TRANSPORT AND GREEN'S FUNCTIONS

In this section, our goal is the analytical evaluation of the total conductance through the QI device depicted in Figs. 1(a) and 1(b). As a matter of fact, solely the spin-up channel contributes to the conductance, once the spin down is energetically inaccessible as previously stated. As our goal is the transport determination around the energy of the MZM, only the bias energy between source and drain leads $|eV| \ll \Delta_{SC} \to \infty$ (infinite superconducting gap standard approximation) is accounted for in the derivation of our conductance expression below [see Ref. [57] and Appendix B]. In the case of a grounded TSC, symmetric QI-lead couplings (Γ) independent of $\mu_{\text{source}} - \mu_{\text{drain}} = eV$, being $\mu_{\text{source}} = -\mu_{\text{drain}} = eV/2$, where e is the elemental charge and V the corresponding bias voltage, the crossed Andreev reflection is suppressed and the conductance can be split into [57]

$$\mathcal{G}_{\text{total}} = \mathcal{G}_{\text{ET}} + \mathcal{G}_{\text{LAR}}, \quad (5)$$

where ET and LAR stand for the electron tunneling and local Andreev reflection processes, respectively, with

$$\mathcal{G}_{\text{ET}}(eV) = \frac{e^2}{2h}\left[\tau_{\alpha\bar{\alpha}}^{\text{ET}}(eV/2) + \tau_{\alpha\bar{\alpha}}^{\text{ET}}(-eV/2)\right], \quad (6)$$

wherein $\alpha = \text{source}$, $\bar{\alpha} = \text{drain}$ and vice versa, together with

$$\mathcal{G}_{\text{LAR}}(eV) = \frac{e^2}{2h}\left[\tau_{\alpha\alpha}^{\text{LAR}}(eV/2) + \tau_{\alpha\alpha}^{\text{LAR}}(-eV/2)\right], \quad (7)$$

in which the transmittances $\tau_{\alpha\bar{\alpha}}^{\text{ET}} = (2S+1)\Gamma^2|\langle\langle d_\uparrow; d_\uparrow^\dagger\rangle\rangle_\omega|^2$ and $\tau_{\alpha\alpha}^{\text{LAR}} = (2S+1)\Gamma^2|\langle\langle d_\uparrow^\dagger; d_\uparrow^\dagger\rangle\rangle_\omega|^2$ are expressed in terms of the frequency-dependent Green's functions (GFs) of type $\langle\langle A_\sigma; B_\sigma\rangle\rangle_\omega = \sum_m \langle\langle A_\sigma|m\rangle\langle m|; B_\sigma\rangle\rangle_\omega$ (details in Appendix A), due to the presence of the large spin, in which the thermal average $\langle|m\rangle\langle m|\rangle = \frac{1}{2S+1}$ should be taken into account. Particularly, these GFs are indeed the time Fourier transform (with $k_B = \hbar = 1$) of

$$\langle\langle A_\sigma; B_\sigma\rangle\rangle_\omega = \int \sum_m \langle\langle A_\sigma(t)|m(t)\rangle\langle m(t)|; B_\sigma(0)\rangle\rangle e^{i\omega^+ t} dt, \quad (8)$$

where $\omega^+ = \omega + i\eta^+$, with $\eta^+ \to 0$ and

$$\langle\langle A_\sigma(t)|m(t)\rangle\langle m(t)|; B_\sigma(0)\rangle\rangle$$
$$= -i\theta(t)\mathcal{Z}^{-1}\mathrm{Tr}\{e^{-\mathcal{H}/T}$$
$$\times [A_\sigma(t)|m(t)\rangle\langle m(t)|, B_\sigma(0)]_+\} \qquad (9)$$

stands for the time-dependent GF following double-brackets Zubarev notation [58], wherein Tr gives the trace over Eq. (1) eigenstates, $\mathcal{Z}$ is the partition function, and $[\ldots, \ldots]_+$ is the anticommutator.

In practice, the GFs should be determined via the standard equation of motion (EOM) approach [59], which in frequency domain, can be summarized as follows:

$$\omega^+\langle\langle A_\sigma; B_\sigma\rangle\rangle_\omega = \langle[A_\sigma, B_\sigma]_+\rangle + \langle\langle[A_\sigma, \mathcal{H}]; B_\sigma\rangle\rangle_\omega. \qquad (10)$$

Additionally, Ref. [57] also ensures that the QI normalized DOS obeys the decomposition

$$\mathrm{DOS}(\uparrow) = -\Gamma\mathrm{Im}\langle\langle d_\uparrow; d_\uparrow^\dagger\rangle\rangle_\omega = \tau_{\alpha\bar\alpha}^{\mathrm{ET}} + \tau_{\alpha\alpha}^{\mathrm{LAR}}. \qquad (11)$$

As Eq. (11) is bounded to unity, it describes the electronic overall transmittance through the QI decomposed into ET and LAR processes, especially when it attains to its maximum value at zero energy, i.e., the $\mathrm{DOS}(\uparrow)(0) = 1$ value gives the electronic zero-frequency spectral weight. In this case, the regular fermionic state of the QI is then made equally by the MZMs γ_A and γ_B. Equivalently, it means that the corresponding normalized DOS for such quasiparticles localize Majorana states with the same spectral weights and, as a result, the QI state is fully built by a pair of resonant MZMs. It gives rise to the conductance $\mathcal{G}_{\mathrm{total}}(0) = \frac{e^2}{h}$. Interestingly enough for $\mathrm{DOS}(\uparrow)(0) = 1/2$, an isolated ordinary MZM is found at the QI site and the zero-bias conductance is characterized by the hallmark $\mathcal{G}_{\mathrm{total}}(0) = \frac{e^2}{2h}$ [3,4]. Such a case corresponds to an ideal infinite superconducting wire. However, there is a regime in which the value $\mathrm{DOS}(\uparrow)(0) = 1/2$ is still present for a finite wire and due to the Ising interaction between the large spin and the QI, the observation of the conductance $\mathcal{G}_{\mathrm{total}}(0) = \frac{e^2}{2h}$ is ensured. This emerges from the excitation that we introduce as the MIQ, in particular, by driving the system into the sweet spot for the exchange interaction J, namely, $J = J_{\mathrm{h}}$. In the latter, the index h stands for the half-fermion special condition of a MZM, which is produced by imposing $\mathrm{DOS}(\uparrow)(0) = 1/2$, from where we extract J_{h} for a given S [see Fig. 3(b)I].

Therefore, to reveal the aforementioned physics about the system conductance, we should begin evaluating Eq. (6) for the ET process. Thus, the GF $\langle\langle d_\uparrow; d_\uparrow^\dagger\rangle\rangle_\omega$ should be found via the EOM method, which gives

$$\langle\langle d_\uparrow; d_\uparrow^\dagger\rangle\rangle_\omega = \frac{1}{2S+1}\sum_m \frac{1}{\omega^+ - \varepsilon_\uparrow - \frac{Jm}{2} + i\Gamma - \Sigma_{\mathrm{MFs}}^{+m}}, \qquad (12)$$

where $\Sigma_{\mathrm{MFs}}^{+m} = K_+ + (2t\Delta)^2 K_{\mathrm{MFs}}\tilde{K}_m$ represents the self-energy correction due to the couplings of the QI with the TSC and the large spin S. This also depends on the following

defined quantities:

$$K_{\mathrm{MFs}} = \frac{\omega^+}{\omega^2 - \varepsilon_M^2 + 2i\omega\eta^+ - (\eta^+)^2}, \qquad (13)$$

$$K_\pm = \frac{\omega^+(\Delta^2 + t^2) \pm \varepsilon_M(t^2 - \Delta^2)}{\omega^2 - \varepsilon_M^2 + 2i\omega\eta^+ - (\eta^+)^2}, \qquad (14)$$

and

$$\tilde{K}_m = \frac{K_{\mathrm{MFs}}}{\omega^+ + \varepsilon_\uparrow + \frac{Jm}{2} + i\Gamma - K_-}. \qquad (15)$$

Concerning the LAR, the conductance of Eq. (7) needs the evaluation of the anomalous GF $\langle\langle d_\uparrow^\dagger; d_\uparrow^\dagger\rangle\rangle_\omega$ instead. After performing the EOM approach, it gives rise to

$$\langle\langle d_\uparrow^\dagger; d_\uparrow^\dagger\rangle\rangle_\omega = -\frac{1}{2S+1}\sum_m \frac{2t\Delta K_m}{\omega^+ + \varepsilon_\uparrow + \frac{Jm}{2} + i\Gamma - \Sigma_{\mathrm{MFs}}^{-m}}, \qquad (16)$$

with $\Sigma_{\mathrm{MFs}}^{-m} = K_- + (2t\Delta)^2 K_{\mathrm{MFs}}K_m$ and

$$K_m = \frac{K_{\mathrm{MFs}}}{\omega^+ - \varepsilon_\uparrow - \frac{Jm}{2} + i\Gamma - K_+}. \qquad (17)$$

However, if we want to know about the possibility of isolating MZMs in the QI, the DOS for γ_A and γ_B should be found to examine the emergence of resonant states. To this end, we invert Eq. (4) for γ_A and γ_B, namely, $\gamma_A = (d_\uparrow^\dagger + d_\uparrow)/\sqrt{2}$ and $\gamma_B = i(d_\uparrow^\dagger - d_\uparrow)/\sqrt{2}$, and we calculate the GFs $\langle\langle\gamma_A; \gamma_A\rangle\rangle_\omega$ and $\langle\langle\gamma_B; \gamma_B\rangle\rangle_\omega$. Consequently,

$$\langle\langle\gamma_j; \gamma_j\rangle\rangle_\omega = \frac{1}{2}[\langle\langle d_\uparrow; d_\uparrow^\dagger\rangle\rangle_\omega + \langle\langle d_\uparrow^\dagger; d_\uparrow\rangle\rangle_\omega$$
$$+ \epsilon(\langle\langle d_\uparrow^\dagger; d_\uparrow^\dagger\rangle\rangle_\omega + \langle\langle d_\uparrow; d_\uparrow\rangle\rangle_\omega)], \qquad (18)$$

where $j = (A, B)$ corresponds to $\epsilon = (+1, -1)$, respectively. Physically speaking, the sign reversal in ϵ can lead to distinct quantum interference phenomena, in particular, between those encoded by the normal GFs ($\langle\langle d_\uparrow; d_\uparrow^\dagger\rangle\rangle_\omega$ and $\langle\langle d_\uparrow^\dagger; d_\uparrow\rangle\rangle_\omega$) and the corresponding superconducting ($\langle\langle d_\uparrow^\dagger; d_\uparrow^\dagger\rangle\rangle_\omega$ and $\langle\langle d_\uparrow; d_\uparrow\rangle\rangle_\omega$). To reveal such interference processes, we need just to find the GFs $\langle\langle d_\uparrow^\dagger; d_\uparrow\rangle\rangle_\omega$ and $\langle\langle d_\uparrow; d_\uparrow\rangle\rangle_\omega$ to close the evaluation of $\langle\langle\gamma_A; \gamma_A\rangle\rangle_\omega$ and $\langle\langle\gamma_B; \gamma_B\rangle\rangle_\omega$. By applying the EOM method, we conclude that

$$\langle\langle d_\uparrow^\dagger; d_\uparrow\rangle\rangle_\omega = \frac{1}{2S+1}\sum_m \frac{1}{\omega^+ + \varepsilon_\uparrow + \frac{Jm}{2} + i\Gamma - \Sigma_{\mathrm{MFs}}^{-m}} \qquad (19)$$

and

$$\langle\langle d_\uparrow; d_\uparrow\rangle\rangle_\omega = -\frac{1}{2S+1}\sum_m \frac{2\Delta t\tilde{K}_m}{\omega^+ - \varepsilon_\uparrow - \frac{Jm}{2} + i\Gamma - \Sigma_{\mathrm{MFs}}^{+m}}. \qquad (20)$$

Naturally, we define the normalized DOS for γ_A and γ_B such as

$$\mathrm{DOS}(\uparrow)[\gamma_j] = -\Gamma\mathrm{Im}\langle\langle\gamma_j; \gamma_j\rangle\rangle_\omega. \qquad (21)$$

This formula elucidates that when the quantity $\mathrm{DOS}(\uparrow)[\gamma_j](0) = -\Gamma\mathrm{Im}\langle\langle\gamma_j; \gamma_j\rangle\rangle_\omega(0) = 1$ is fulfilled, it

can be recognized as the maximum Majorana quasiparticle transmittance or its corresponding zero-frequency spectral weight.

Henceforward, we focus attention on the case $\varepsilon_\uparrow = 0$ (grounded SC). We perceive by inspecting Eqs. (12) and (19) that Eq. (11) becomes also DOS$(\uparrow) = -\Gamma \text{Im}\langle\langle d_\uparrow^\dagger; d_\uparrow \rangle\rangle_\omega$. Additionally, $-\Gamma \text{Im}\langle\langle d_\uparrow^\dagger; d_\uparrow^\dagger \rangle\rangle_\omega = -\Gamma \text{Im}\langle\langle d_\uparrow; d_\uparrow \rangle\rangle_\omega$. This, in combination with Eqs. (18) and (21), allows us to establish that

$$\text{DOS}(\uparrow) = \tfrac{1}{2}(\text{DOS}(\uparrow)[\gamma_A] + \text{DOS}(\uparrow)[\gamma_B]). \quad (22)$$

Consequently, by taking into account this finding together with Eqs. (5), (6), (7), and (11), we conclude the providential equality as follows:

$$\mathcal{G}_{\text{total}} = \mathcal{G}_{\gamma_A} + \mathcal{G}_{\gamma_B}, \quad (23)$$

where

$$\mathcal{G}_{\gamma_j}(\text{eV}) = \frac{e^2}{4h}[\text{DOS}(\uparrow)[\gamma_j](\text{eV}/2) + \text{DOS}(\uparrow)[\gamma_j](-\text{eV}/2)] \quad (24)$$

stands for the conductance contribution arising from the quasiparticle γ_j within the QI.

We highlight that Eq. (23) introduces an alternative perspective concerning the underlying physics of the conductance in Eq. (5): the ET and LAR quantum transport mechanisms are revealed as the net effect of two Majorana quasiparticle conductances, namely, the corresponding contributions arising from γ_A and γ_B, respectively. In this context, our main findings hold for the constraint $J = J_\text{h}$ fulfilled, thus characterizing the system sweet spot to produce the MIQ. This regime consists of the maximum Majorana quasiparticle transmittance DOS$(\uparrow)[\gamma_j](0) = 1$, surprisingly, fractionalized and split into DOS$(\uparrow)[\gamma_A](0) = 1/2$ and DOS$(\uparrow)[\gamma_B](0) = 1/2$. Despite such equipartition, the electronic transmittance is still given by DOS$(\uparrow)(0) = 1/2$ [see Fig. 3(b)I] and, according to Eq. (24), it ensures $\mathcal{G}_{\gamma_A}(0) = \frac{e^2}{4h}$ and $\mathcal{G}_{\gamma_B}(0) = \frac{e^2}{4h}$. However, counterintuitively, solely $\mathcal{G}_{\gamma_B}(0)$ contains a MZM in the common sense, i.e., a resonant state, while $\mathcal{G}_{\gamma_A}(0)$ shows a dip instead, but with the same magnitude of the peak in γ_B. This is the reason we call the contribution $\mathcal{G}_{\gamma_B}(0) = \frac{e^2}{4h}$ by $\mathcal{G}_{\text{MIQ}}(0)$ with attention to the emergent MIQ. This is the unique MZM-type resonant state that appears in the system due to the interplay between the topological superconductivity and the Ising Hamiltonian. In this case, Eqs. (5) and (23) ensure that when the MIQ emerges, $\mathcal{G}_{\gamma_B}(0)$ exhibits a maximum and $\mathcal{G}_{\gamma_A}(0)$ shows a minimum, in such a way that only $\mathcal{G}_{\text{ET}}(0)$ enters into $\mathcal{G}_{\text{total}}(0) = \frac{e^2}{2h}$. It means that the LAR process is found entirely suppressed within this regime. The complete analysis here summarized will be discussed in the next section.

IV. RESULTS

In the entire numerical analysis of Sec. IV A, we keep constant $\varepsilon_\uparrow = 0$ (grounded SC), $\lambda_1 = 2.12\Gamma$ ($\Delta = t$) and perform variations in the parameters ε_M, S and J. Partially for Sec. IV B, we assume $|\lambda_1| \sim |\lambda_2|$ [$\Delta \neq 0, t \to 0$] from Eq. (1) [Eq. (3)] to analyze the ABSs regime within the

framework of the effective model [33]. We should remember that $\mu_{\text{source}} - \mu_{\text{drain}} = \text{eV}$ represents the bias energy between source and drain leads, with the choice $\mu_{\text{source}} = -\mu_{\text{drain}} = \text{eV}/2$ in our transport calculations.

A. Majorana-Ising-type quasiparticle excitation

In Fig. 2, we present, for the QI of Fig. 1, the total conductance of Eq. (5) as a function of the bias-voltage eV/Γ. Particularly, in Fig. 2(a) the ideal case is considered, i.e., the TSC wire is perfectly infinite ($\varepsilon_M = 0$) and the large spin is found turned off ($S = 0$). This case is well-known, being characterized by the ZBP in the conductance given by $\mathcal{G}_{\text{total}}(0) = \frac{e^2}{2h}$ [3,4]. Interestingly enough, this ZBP in the conductance represents the isolated MZM γ_1 originally attached to one edge of the TSC wire, which leaks towards the QI site in the form of the MZM γ_A. The MZM leakage from the TSC edge into the QI is then characterized by the DOS$(\uparrow)[\gamma_A](0) = 1$ and DOS$(\uparrow)[\gamma_B](0) = 0$. We will provide extra details concerning this issue in the discussion of Fig. 3(a)I. On the other hand, the satellite peaks in Fig. 2(a) are the aftermath of the splitting arising from the condition $i\sqrt{2}\lambda_1\gamma_B\gamma_1$ given by Eq. (3) for the poor man's Majorana regime of the system [55,56]. Additionally, we have made explicit via Eq. (5) that the ET and LAR processes compose the total conductance. Thus, such a feature can be viewed in Fig. 2(b), where we note, in particular, for the ZBP conductance that, the ET and LAR split equally. Here we propose that it is still achievable to obtain $\mathcal{G}_{\text{total}}(0) = \frac{e^2}{2h}$ for a finite TSC wire and to also perform the isolation of a Majorana quasiparticle at the QI site. In our setup, such an excitation rises, in particular, dressed by the Ising interaction. To this end, an integer large spin S should be accounted for and be coupled to the QI with a special value in the exchange interaction J. Thus, by evaluating $J = J_\text{h}$, the amplitude $\mathcal{G}_{\text{total}}(0) = \frac{e^2}{2h}$ [Eq. (23)] finally becomes restored. However, we will verify that such a configuration corresponds to isolate a peculiar MZM, namely, γ_B, with a resonant peak characterized by the spectral weight DOS$(\uparrow)[\gamma_B](0) = 1/2$ [Eq. (21)], while for γ_A we have the same amplitude, i.e., DOS$(\uparrow)[\gamma_A](0) = 1/2$, but with a dip instead.

Now, we consider the presence of a large spin S. Figures 2(c) and 2(d) show the total conductance in the presence of $S = 3$ and $J_\text{h} = 1.335\Gamma$ [Fig. 3(b)I] for a finite TSC with $\varepsilon_M = \Gamma$. The ZBP conductance in Fig. 2(c) is $\mathcal{G}_{\text{total}}(0) = \frac{e^2}{2h}$ as expected, but the decomposition into ET and LAR channels described in Fig. 2(d) reveals a striking result: solely ET survives, while LAR is completely suppressed at zero bias. Below we will verify that the LAR suppression corresponds to a quasiparticle localization in the DOS for γ_B, which leads to DOS$(\uparrow)[\gamma_B](0) = 1/2$. Thus, according to Eq. (24), such a finite DOS contributes to a conductance $\mathcal{G}_{\gamma_B}(0) = \mathcal{G}_{\text{MIQ}}(0) = \frac{e^2}{4h}$, where we define the MIQ $\gamma_B \equiv \gamma_{\text{MIQ}}$.

To understand the emergence of the MIQ, we begin with the trivial case in Fig. 3(a): The central panel discriminates the electronic DOS$(\uparrow)$ into the corresponding DOS for γ_A and γ_B [Eq. (21)] with $S = 0$ and $\varepsilon_M = \Gamma$. This case is regarded as trivial once we verify that in both DOS, γ_A and γ_B resonant states pinned at zero energy $\omega = 0$ are present. Schematically, the QI fermionic state can be imagined as a sphere formed

by two MZMs depicted by two calottes. This is the manner in which we outline pictorially the two zero-energy resonant states, the so-called MZMs in the DOS γ_A and γ_B. This sketch can be found in the upper-right inset of Fig. 3(a), in which each calotte symbolizes the half-fermionic character of the MZM. Equivalently, a calotte occupies the half volume of the sphere and as it corresponds to a MZM, it can be surely characterized by DOS$(\uparrow)[\gamma_j](0) = 1$. As aftermath, according to Eqs. (22)–(24), these two MZMs lead to the zero-bias conductance peak $\mathcal{G}_{\text{total}}(0) = \frac{e^2}{h}$. Concerning the satellite peaks in the DOS$(\uparrow)[\gamma_B]$, they occur due to the overlap between the MZMs γ_B and γ_1. On the other hand, Fig. 3(a)II shows the spin-down channel, which is the one decoupled from the TSC. To analyze it on the same footing as the spin-up channel, we assume artificially $\varepsilon_\downarrow = 0$ and verifies that both the MZMs γ_C and γ_D, which constitute this spin sector of the QI, are then identified exactly by degenerate resonant states. The evaluation of the DOS for the spin-down sector just employs the GFs for the spin-up sector, but it disregards the superconducting terms. As none of these MZMs overlap with γ_1, a full superposition of the line shapes for these MZMs manifests in the profiles of the DOS γ_C and γ_D. Therefore, satellite peaks do not emerge. Now, let us go back to discuss the spin-up channel. We should pay particular attention to the case $\varepsilon_M = 0$ depicted in Fig. 3(a)I, which corresponds to the nonoverlapped situation between γ_1 and γ_2. This scenario is the ideal one and it contains the pillars for the conductance behavior of Fig. 2(a). Note that γ_B overlaps with γ_1, leading to satellite peaks in DOS$(\uparrow)[\gamma_B]$ and DOS$(\uparrow)[\gamma_B](0) = 0$, while γ_A is found isolated and localized as a well-defined resonant zero mode with spectral weight DOS$(\uparrow)[\gamma_A](0) = 1$. Thereafter, $\mathcal{G}_{\text{total}}(0) = \mathcal{G}_{\gamma_A}(0) = \frac{e^2}{2h}$. This case is well-known in literature [3,4] and points out that the MZM γ_A contributes to the conductance as a resonant state in contrast to γ_B, which shows a gap in DOS$(\uparrow)[\gamma_B]$ around zero bias. This latter prevents a finite conductance, i.e., $\mathcal{G}_{\gamma_B}(0) = 0$. Below, we will see that by turning on the exchange J for a given S, the spectral profiles for the DOS$(\uparrow)[\gamma_A]$ and DOS$(\uparrow)[\gamma_B]$ will exhibit a multilevel structure. Additionally, these densities will be responsible, according to Eq. (24), by a nonquantized $\mathcal{G}_{\text{total}}(0) \neq \frac{e^2}{h}$ in Eq. (23). In the situation of arbitrary J, the contributions to $\mathcal{G}_{\text{total}}(0) \neq 0$ will not arise from well-defined resonant zero-mode states in DOS$(\uparrow)[\gamma_A]$ and DOS$(\uparrow)[\gamma_B]$. The Majorana fermion localization within the QI as a resonant zero-mode state will only occur for the sweet spot $J = J_{\text{h}}$.

Figure 3(b) treats the presence of a large spin coupled to the QI for $\varepsilon_M = \Gamma$. As we can see, the Ising interaction $J = 5\Gamma$ for $S = 3$ clearly affects the spectral profiles of DOS$(\uparrow)[\gamma_A]$ and DOS$(\uparrow)[\gamma_B]$. Basically, it introduces a multilevel structure for the satellite peaks and modifies drastically the MZM localization around the zero-bias. Surprisingly, the DOS$(\uparrow)[\gamma_A]$ presents a valley (dip) at zero energy and a quasiresonant MZM rises in DOS$(\uparrow)[\gamma_B]$. As a matter of fact, the latter cannot be considered a well-defined resonant MZM: its spectral weight is not exactly an integer or semi-integer number, and the line-shape broadening does not obey a *Lorentzian-like* form. The line shapes of such spectral densities are then distinct, but counterintuitively, their zero-bias values coincide, i.e., DOS$(\uparrow)[\gamma_A](0) = $ DOS$(\uparrow)[\gamma_B](0)$.

As the spin-up sector of the QI is the one coupled to the TSC, the spectral profiles in the DOS$(\uparrow)[\gamma_A]$ and DOS$(\uparrow)[\gamma_B]$ do not strictly follow the standard angular momentum theory for the Zeeman splitting [Eq. (2)]. Usually, this theory ensures that for an integer S, $2S$ symmetrically displaced levels around the corresponding $\omega = \varepsilon_\uparrow = 0$ should emerge. Here, indeed we observe a mirror-symmetric set with S energy bands below and above the zero bias, respectively, where nearby peculiar spectral structures rise. We reveal that the profiles differ significantly in this range, as aftermath of the nontrivial interplay between the TSC and Ising exchange term. In Figs. 4(d)–4(f), we will see that the manifestation of this effect lies within a region comprised by *cone-like walls* spanned by ω and ε_M in the DOS of the system. Within the cone, the Zeeman splitting becomes unusual and the energy spacing between the levels is simultaneously governed by J and ε_M. In addition, solely the spin-down channel shows standard Zeeman splitting, once it does not perceive the TSC. This can be verified in Fig. 3(b)II, where the DOS for γ_C and γ_D, as expected, present the ordinary $2S + 1$ multilevel structure ensured by Eq. (2). We highlight that upon decreasing the exchange parameter J, the restoration of the conductance $\mathcal{G}_{\text{total}}(0) = \frac{e^2}{2h}$ can still be allowed. Thus, we should remember that such a conductance arises from the fulfillment of the condition DOS$(\uparrow)(0) = 1/2$. Particularly, in Fig. 3(b)I, we show exactly the points where this happens by considering several values of S and $\varepsilon_M \neq 0$. Particularly, for $S = 3$, this sweet spot occurs for $J = J_{\text{h}} = 1.335\Gamma$ and its dependence on ε_M is revealed as very weak, according to our numerical calculations (not shown). It means that $J = J_{\text{h}} = 1.335\,\Gamma$ still keeps the value DOS$(\uparrow)(0) = 1/2$ while ε_M does not exceed very much Γ ($\varepsilon_M \gg \Gamma$). Experimentally speaking, J can be tuned by changing the tip-QI vertical distance. Thus, for $\varepsilon_M \neq 0$, $\mathcal{G}_{\text{total}}(0)$ drops from $\frac{e^2}{h}$ to $\frac{e^2}{2h}$ when $J = J_{\text{h}}$. Hence, at the sweet spot, if one knows previously the spin S of the tip, J_{h} can be extracted from Fig. 3(b)I or vice versa.

In Fig. 3(c), we present the case $J = J_{\text{h}} = 1.335\Gamma$ that leads to our main finding: a localization of a resonant state at zero energy in DOS$(\uparrow)[\gamma_B]$, with spectral weight DOS$(\uparrow)[\gamma_B](0) = 1/2$. The latter amplitude points out that the ordinary MZM now is fractionalized and the value DOS$(\uparrow)[\gamma_B](0) = 1$ is not present anymore. This fractionalized MZM, which we call MIQ, then leads to a conductance $\mathcal{G}_{\gamma_B}(0) = \mathcal{G}_{\text{MIQ}}(0) = \frac{e^2}{4h}$ as ensured by Eq. (24). The value DOS$(\uparrow)[\gamma_B](0) = 1/2$ can be pictorially viewed by the half calotte found in the lower-right inset of Fig. 3(c), which symbolizes the MZM fractionalization within the QI state. Nevertheless, to complete the total conductance $\mathcal{G}_{\text{total}}(0) = \frac{e^2}{2h}$, the zero-bias value for DOS$(\uparrow)[\gamma_A](0)$ should coincide, i.e., DOS$(\uparrow)[\gamma_A](0) = 1/2$ and, as aftermath, $\mathcal{G}_{\gamma_A}(0) = \frac{e^2}{4h}$ as well. Here we emphasize that in DOS$(\uparrow)[\gamma_A](0)$ a quantum destructive interference manifests and a resonant state does not rise at zero bias. Moreover, it is capital to clarify the underlying mechanism to produce the MIQ: the key idea is the decrease of J, thus forcing the merge of the $2S$ side bands (satellite peaks) of the system towards the zero energy, where a resonant level is pinned. As a result, this sum of amplitudes for the satellite peaks interferes constructively at zero energy, giving rise to DOS$(\uparrow)(0) = 1/2$ for $J = J_{\text{h}}$. Further,
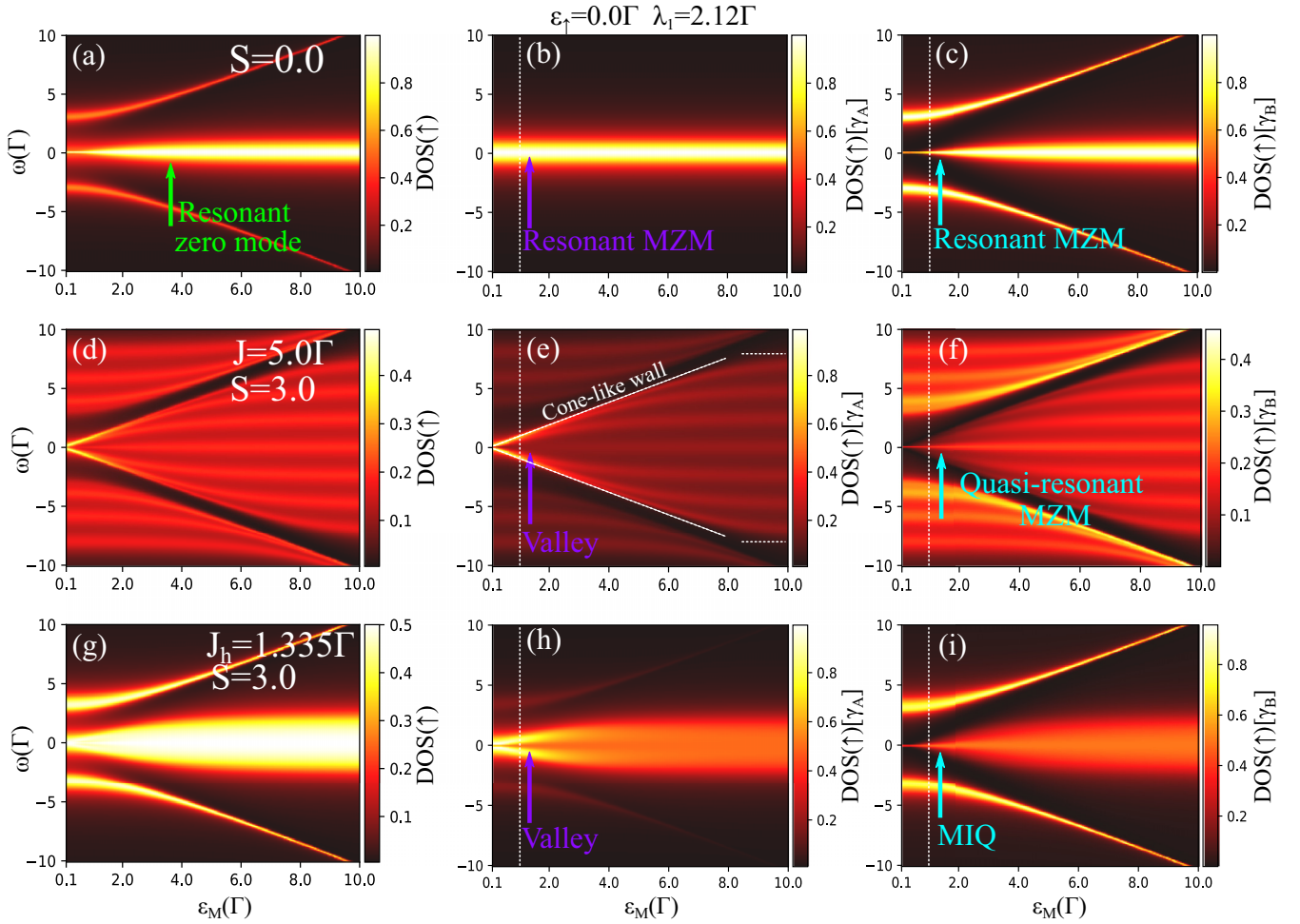
FIG. 4. Color maps of Eqs. (11) and (21) for the QI, γ_A and γ_B DOS, respectively, spanned by the frequency ω and ε_M: (a) In the case $S = 0$, the ZBP in the DOS($\uparrow$) arises from the individual ZBPs found in DOS($\uparrow$)[γ_A] [panel(b)] and DOS($\uparrow$)[γ_B] [panel(c)], due to the MZMs γ_A and γ_B that act as the building blocks of the QI state $\varepsilon_\uparrow = 0$ [Eq. (22)]. They reveal that the system does not contain isolated MZMs and that the overlapped γ_1 and γ_2 split the zero-mode energy state leading to the upper and lower arcs in (a) and (c). (d)–(f) reveal the influence of $S = 3$ and $J = 5\Gamma$ on the QI, where we can clearly see a $2S + 1$ multilevel structure centered at $\omega = 0$. The upper and lower arcs, distinctly, show $2S$ levels each. The central region of (e) has a valley-type structure in contrast to that for (f), which points out a quasiresonant MZM. In both cases, the $2S + 1$ multilevel structure is delimited by cone-like walls up to a threshold in ε_M (not indicated), where above it the DOS($\uparrow$)[γ_A] and DOS($\uparrow$)[γ_B] exhibit a zero mode with the lines of the walls parallel to each other. For this situation, the TSC plays no role and the MZMs γ_A and γ_B stay paired as in (a)–(c). (g)–(i) hold for the sweet spot $J = J_h = 1.335\Gamma$, where we have the zero-frequency valley and peak well-resolved in the DOS($\uparrow$)[γ_A] and DOS($\uparrow$)[γ_B], respectively. In the latter, the MIQ rises as aftermath of the partial merge of the $2S + 1$ multilevel structure centered at $\omega = 0$ upon decreasing the coupling J. We call attention to the vertical lines, which represent slice cuts of the cases profoundly explored in Figs. 2 and 3.

our findings do not depend on the sign of J and in case of a semi-integer large spin, the multilevel structure is even and a zero energy is absent in the spectrum. In this manner, the MIQ cannot be excited. Concerning Figs. 3(c)I and 3(c)II, we verify that for $\varepsilon_M \gg \Gamma$ (or $\varepsilon_M \to \infty$) the DOS for the Majorana fermions are degenerate. For extremely short TSC wires ($\varepsilon_M \to \infty$), the energy level ε_M for the orbital f [Eq. (3)] is highly off resonance of the QI energy $\varepsilon_\uparrow = 0$, thus making the QI and TSC decouple from each other. Thus, the spin-up channel behaves as the corresponding spin down, which is the one permanently decoupled from the TSC. This implies that the MIQ cannot be seen for very short wires.

Figure 4 summarizes our findings exhibiting color maps of Eqs. (11) and (21) for the electronic and Majorana

DOS, respectively, and spanned by ω and ε_M. Figures 4(a)–4(c) describe the case $S = 0$, which is characterized by DOS($\uparrow$)(0) = 1 and DOS($\uparrow$)[γ_A](0) = DOS($\uparrow$)[γ_B](0) = 1. This corresponds to the trivial regime where two MZMs localize around zero bias and appear at the QI site. Such a characteristic lies on the ZBPs and appears as horizontal lines in the representation of Figs. 4(a)– 4(c) for any finite value of ε_M. As we can see, the satellite peaks in Fig. 4(a) arise from Fig. 4(c). By turning on the Ising interaction with $S = 3$ and $J = 5\Gamma$, the spectral profiles of the DOS acquire distinct patterns: the satellite peaks obey approximately the standard angular momentum theory for the Zeeman splitting, thus exhibiting $2S$ split sidebands. In this situation, the linear dependence on the exchange parameter J is lacking. In

addition, the central regions of Figs. 4(a)– 4(c) are converted into the domains delimited by *cone-like walls* as those found in Figs. 4(d)–4(f). While these walls persist up to a threshold in ε_M (not marked in the figures), a sophisticated interplay between the TSC and the Ising interaction rules the physics of the system and allows the possibility of the MIQ existence. Note that for $\varepsilon_M > \Gamma$, a $2S + 1$ multilevel central structure finally becomes resolved. It is worth mentioning that for $\varepsilon_M = \Gamma$, the line cuts in Fig. 4 given by the vertical dashed lines then correspond to the cases discussed in detail in Fig. 3. We would like to mention that the choice $\varepsilon_M = \Gamma$ corresponds to a strong limit, just to better resolve our findings. However, while ε_M stays within the aforementioned *cone-like walls,* the effect persists. In Figs. 4(e) and 4(f), we note the rising of the valley and the quasiresonant MZM spectral structures, respectively, upon increasing ε_M. However, much above the threshold in ε_M, the linear spacing in J for the Zeeman splitting is restored and this situation is that delimited by the marked horizontal dashed lines. Finally, Figs. 4(g)–4(i) show the merge of the multilevel structure in the sweet spot $J = J_h = 1.335\Gamma$, leading to the emergence of the MIQ in the Majorana channel γ_B, while the valley continues in the channel γ_A. Therefore, within *the cone-like wall* domain, the sector γ_B of Majorana fermions for the QI makes explicit a constructive interference process at zero bias, while the corresponding in γ_A displays a destructive behavior. In this regime, the conductance $\mathcal{G}_{LAR}(0)$ becomes fully quenched and just $\mathcal{G}_{ET}(0)$ contributes to $\mathcal{G}_{total}(0) = \frac{e^2}{2h}$ [Fig. 2(d)].

B. Poor man's Majoranas, parity qubit, and ABS regime

In this section, we clarify that the MIQ excitation can be classified as a poor man's Majorana [55,56] and, to demonstrate such, the analysis of the DOS for the MZMs of Eq. (3) placed at the Kitaev dimer right edge is performed. To accomplish this goal, we employ pertinent GFs from Appendix C. Additionally, we discuss the possibility of having a MIQ excitation-based parity qubit for quantum computing purposes [55] and the ABSs regime within the effective model of Eq.(1) [33]. To this end, let us focus again on the left edge of the Kitaev dimer, i.e., the QI. This system part description is found in the central panel of Fig. 3(a) ($\varepsilon_M = \Gamma$) and its inset, Fig. 3(a)I ($\varepsilon_M = 0$), which account for the QI operator $d_\uparrow$, where the MZMs γ_A and γ_B reside [Eq. (4)]. Particularly, these panels show two resonant and single MZMs, respectively, while in Fig. 5(a), a resonant MZM appears permanently in the DOS $(-1/\pi)\mathrm{Im}\langle\langle\gamma_2;\gamma_2\rangle\rangle_\omega$ (not normalized, once leads are lacking at this side) for γ_2 in both the situations, thus describing the MZM placed at the TSC right edge. Such a characteristic is entirely understood within the theoretical framework for the Kitaev dimer described in Ref. [55]. The latter points out that systems based on Eq. (3) for QIs tunnel and are Andreev coupled, which in our case are given by the $d_\uparrow$ and f orbital sites, and could contain the so-called poor man's Majorana. These MZMs, in particular, cannot be considered topologically protected as true MZMs, and emerge at the Leijnse and Flensberg sweet spot [55] when the following set of parameters is obeyed: $J = 0$, $\Delta = t$ and $\varepsilon_M = \varepsilon_\uparrow = 0$. This scenario can be observed in Figs. 3(a)I and 5(a)I, which reveal resonant MZMs, namely, the poor man's Majorana,
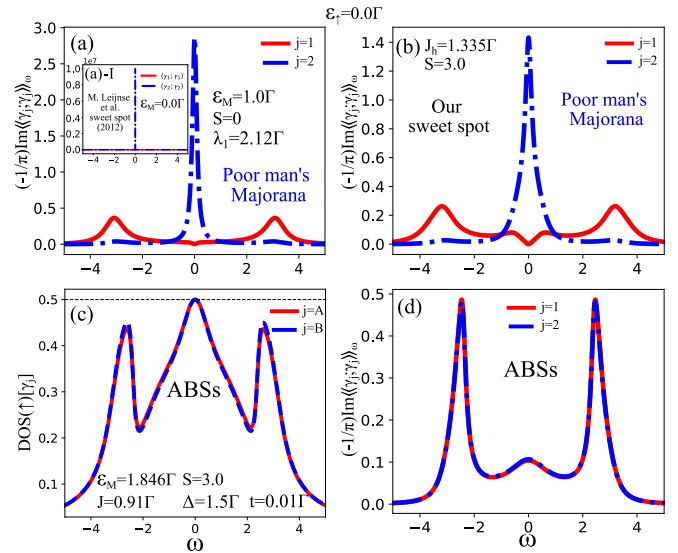
FIG. 5. (a) and (b) show Leijnse and Flensberg [55] and our sweet spots, respectively, for poor man's Majoranas. The Andreev bound state (ABS) regime of Refs. [33,34] appear depicted in (c) and (d). Additionally, fractionalization of zero modes also occurs in the latter.

with one placed at the left and the other at the right of the Kitaev dimer. This statement holds, since the spectral weights are given by the $DOS(\uparrow)[\gamma_A](0) = 1$ and $DOS(\uparrow)[\gamma_B](0) = 0$ for the QI [Fig. 3(a)I], while we have $DOS[\gamma_1](0) = 0$ and $DOS[\gamma_2](0) \neq 0$ for the Kitaev dimer's right edge, as depicted in the inset of Fig. 5(a). For the aforementioned case, the nonlocal fermion $\eta = (\gamma_A - i\gamma_2)/\sqrt{2}$ can be made via the linear combination between the resonant MZMs γ_2 and γ_A localized at the right and left of the dimer, respectively [55]. In this manner, the fermion parity, which is given by the electronic occupation of $\eta^\dagger\eta$, becomes a feasible quantity for quantum computing [55]. For the resonant MZMs γ_A and γ_B at the left, depicted in the central panel of Fig. 3(a) and the corresponding Fig. 5(a), i.e., the situation off the Leijnse and Flensberg sweet spot with $\varepsilon_M = \Gamma$, the fragility of these poor man's Majoranas becomes evident. In such a case, the spectral weights $DOS(\uparrow)[\gamma_A](0) = 1$ and $DOS(\uparrow)[\gamma_B](0) = 1$ occur simultaneously at the QI. Thus, according to Ref. [55], the zero-mode dip in the DOS $(-1/\pi)\mathrm{Im}\langle\langle\gamma_1;\gamma_1\rangle\rangle_\omega$ represents the spill of the MZM γ_1 from the f orbital site over the QI, being characterized by the $DOS(\uparrow)[\gamma_B](0) = 1$. As aftermath, these two resonant MZMs inevitably introduce an ambiguous definition for the nonlocal parity qubit, i.e., it could be $\eta = (\gamma_A - i\gamma_2)/\sqrt{2}$ or $\eta = (\gamma_B - i\gamma_2)/\sqrt{2}$. In this way, the parity qubit becomes not well-defined and its employment compromised, as expected, for quantum computing.

With this in mind, we back to our sweet spot in Fig. 3, where the Ising term J_h, by considering $\varepsilon_M = \Gamma$, siphons off the $DOS(\uparrow)[\gamma_A](0) = 1$ [Fig. 3(a)] from resonant profile towards one antiresonant with $DOS(\uparrow)[\gamma_A](0) = 1/2$ [Fig. 3(c)], while it keeps the $DOS(\uparrow)[\gamma_B = \gamma_{MIQ}](0) = 1/2$ [Fig. 3(c)] resonant after such a deviation from the value $DOS(\uparrow)[\gamma_B](0) = 1$ [Fig. 3(a)]. As the MZM given by γ_{MIQ} exhibits resonant character and its partner γ_A is of antiresonant

type, it means that the QI does not host exactly one MZM. It is an indication that a MZM is spilled over the QI from the f orbital site, where the DOS$[\gamma_1](0) = 0$ and the resonant DOS$[\gamma_2](0) \neq 0$ still persist, as can be seen in Fig. 5(b). Thus, such features reinforce that the MIQ excitation obeys the properties of the poor man's Majorana [55]. Let us remember that in Figs. 3(a)I and 5(a)I, the left and right resonant MZMs were linearly combined to build η when $\varepsilon_M = 0$. However, an extrapolation to $\eta = (\gamma_{\text{MIQ}} - i\gamma_2)/\sqrt{2}$ for $\varepsilon_M \neq 0$ instead, despite being $\gamma_B = \gamma_{\text{MIQ}}$ resonant and γ_A not, deserves further investigation, once Ref. [55] does not cover such a limit. We leave the advances on this particular parity qubit issue to better exploration elsewhere, since they do not belong to the scope of our current research. We call attention to our main findings, which consist of showing one way of realizing the fractionalization of MZMs, in particular, via the Ising coupling to a QI site.

Still concerning the nature of the fractionalized spectral weight peak given by DOS$(\uparrow)[\gamma_{\text{MIQ}}](0) = 1/2$, we attribute its origin to several modes that, added up, result in a half-integer contribution. Indeed, each mode, as we know, due to the QI-leads coupling, becomes a band centered at the mode in the absence of the leads. As the separation between the modes (centers of these bands) depends directly on the Ising coupling J, by decreasing to $J = J_h$ (our sweet spot), it favors the partial merge of the $2S + 1$ odd number of bands at zero energy, where there is an accumulation point. This is naturally imposed by the choice of an integer S. Consequently, we find the peak DOS$(\uparrow)[\gamma_{\text{MIQ}}](0) = 1/2$ and the dip DOS$(\uparrow)[\gamma_A](0) = 1/2$, when we fix DOS$(\uparrow)(0) = 1/2$ in Eq. (22).

In summary, as we demonstrated, the MIQ excitation (the resonant one) and γ_A (the corresponding partner antiresonant) at the system left, together with γ_2 at right, are poor man's Majoranas, since they obey their properties of partially protection (not topological) introduced by Ref. [55]. It is worth mentioning that poor man's Majoranas were recently verified in the experiment of Ref. [56] and, in our case, the poor man's Majorana observed at the QI show a fractionalized characteristic, due to the Ising coupling. At the Leijnse and Flensberg sweet spot [55], the Ising term plays no role and we still have DOS$(\uparrow)(0) = 1/2$, but with the DOS$(\uparrow)[\gamma_B](0) = 0$ and a peak in the DOS$(\uparrow)[\gamma_A](0) = 1$, thus reflecting not fractionalized MZMs. In both sweet spots, it is capital to note that we have always $\mathcal{G}_{\text{total}}(0) = \frac{e^2}{2h}$, once we adopt the right side of Eq. (4) as the basis for the quasiparticle excitations of the electron at the QI [Eq. (11)]. This basis is convenient to evaluate the system quantum transport and elucidates if just one MZM (Leijnse and Flensberg sweet spot) or half of each from the MZM couple of the quasiparticle excitations at the QI (our sweet spot), is really contributing to $\mathcal{G}_{\text{total}}(0) = \frac{e^2}{2h}$.

Figures 5(c) and 5(d) discuss the ABS regime, which can be captured by imposing $|\lambda_1| \sim |\lambda_2|$ [$\Delta \neq 0$, $t \to 0$] in Eq. (1) [Eq. (3)], as pointed out by Ref. [33]. It is worth mentioning that such a scenario corresponds to place the MZMs γ_1 and γ_2 practically at the same TSC edge [see Fig. 1(d)], with model parameters marked in Fig. 5(c), from where we highlight $\Delta = 1.5\Gamma$ and $t = 0.01\Gamma$. Thus, it leads to a conductance $\mathcal{G}_{\text{total}}(0) = \frac{e^2}{2h}$, which is purely from ET, but counterintuitively, assisted by Andreev reflection. It means that although

$\mathcal{G}_{\text{LAR}}(\text{eV}) \to 0$ through the QI flanked by the leads [Eqs. (7), (16), and (20)], the Kitaev dimer, indeed still admits Andreev reflection, in particular, between the $d_\uparrow$ and f orbitals given by the terms $\Delta d_\uparrow f + \text{H.c.}$ [Eq. (3), [55]], which then build the quasiparticle electronic state at the QI. As Eqs. (23) and (24) also determine $\mathcal{G}_{\text{total}}(0) = \frac{e^2}{2h}$, in Fig. 5(c), we evaluate then the DOS$(\uparrow)[\gamma_j] = -\Gamma \text{Im}\langle\langle \gamma_j; \gamma_j \rangle\rangle_\omega$ [Eq. (21)], which strongly depend only on the GFs $\langle\langle d_\uparrow; d_\uparrow^\dagger \rangle\rangle_\omega$ and $\langle\langle d_\uparrow^\dagger; d_\uparrow \rangle\rangle_\omega$ [Eq.(18)], since $\langle\langle d_\uparrow; d_\uparrow \rangle\rangle_\omega = \langle\langle d_\uparrow^\dagger; d_\uparrow^\dagger \rangle\rangle_\omega \to 0$ [Eqs. (16) and (20)] in the ABS regime. By looking at Eqs. (A1) and (A2) in Appendix A, we verify that $\langle\langle d_\uparrow; d_\uparrow^\dagger \rangle\rangle_\omega$ and $\langle\langle d_\uparrow^\dagger; d_\uparrow \rangle\rangle_\omega$ have a dependence on $\Delta\langle\langle f^\dagger|m\rangle\langle m|; d_\uparrow^\dagger \rangle\rangle_\omega$ and $\Delta\langle\langle f|m\rangle\langle m|; d_\uparrow \rangle\rangle_\omega$, which are modulated by the SC pairing Δ and GFs associated to $\Delta d_\uparrow f + \text{H.c.}$ for the Andreev process. Such features establish the Andreev reflection between the QI and f, while $\mathcal{G}_{\text{LAR}}(\text{eV}) \to 0$ is evaluated at the interface QI leads. Additionally, we should highlight that similar analysis in observing the ABSs regime, in particular, within the effective model of Eq. (1) but without the Ising term, was already performed by some of us via the analogous Eq. (20) of Ref. [34], and now we extend it to the current Hamiltonian. As consequences, Fig. 5(c) also exhibits the DOS siphon off to 1/2 for γ_A and γ_B, which, distinct from Figs. 5(a) and 5(b) with $\Delta = t$, are identically resonant. In Fig. 5(d), a pair of ABSs manifests too. To conclude, $\mathcal{G}_{\text{total}}(0) = \frac{e^2}{2h}$ could be reproduced by both the poor man's Majoranas and ABS regimes.

V. CONCLUSIONS

We found that the fractionalization of regular MZMs becomes a feasible task once an integer large spin S is exchange coupled to a QI, in particular, when it acts as the new edge of a finite TSC in 1D. A counterintuitive regime arises due to a sweet value for the Ising coupling, which is capable of localizing a fractionalized MZM. We introduce such an excitation as the MIQ. As aftermath, we report the emergence of one MZM with the maximum spectral weight reduced by half and exhibiting resonant character. In contrast, the other MZM mode in the QI does not localize around zero energy, but shows the same spectral weight of the resonant MZM via an antiresonant profile. Interestingly enough, due to the localization of the MIQ, half of the quantum conductance is made essentially by the normal electronic contribution, while that from the Andreev reflection is totally lacking between the QI and leads. This behavior differs from that observed in perfectly infinite TSC wires, in which one MZM localizes at the QI site with maximum spectral weight given by unit and with electronic and Andreev conductances equally split at zero bias. Therefore, our proposal points out a manner to induce, within a more realistic perspective from an experimental point of view, a quantum state at the edge of a short TSC in 1D. Additionally, our MIQ is demonstrated to be a poor man's Majorana [55,56].

APPENDIX A: GREEN'S FUNCTIONS FOR THE SYSTEM'S LEFT SIDE

As the GFs in the presence of the large spin obey the notation $\langle\langle A_\sigma; B_\sigma\rangle\rangle_\omega = \sum_m \langle\langle A_\sigma|m\rangle\langle m|; B_\sigma\rangle\rangle_\omega$ [58], here we make explicit the details in the EOM approach to find the elements of type $\langle\langle A_\sigma|m\rangle\langle m|; B_\sigma\rangle\rangle_\omega$. In what follows, we have

$$\left(\omega^+ - \varepsilon_\uparrow - \frac{Jm}{2} + i\Gamma\right)\langle\langle d_\uparrow|m\rangle\langle m|; d_\uparrow^\dagger\rangle\rangle_\omega$$
$$= \frac{1}{2S+1} - t\langle\langle f|m\rangle\langle m|; d_\uparrow^\dagger\rangle\rangle_\omega - \Delta\langle\langle f^\dagger|m\rangle\langle m|; d_\uparrow^\dagger\rangle\rangle_\omega,$$
$$\text{(A1)}$$

$$\left(\omega^+ + \varepsilon_\uparrow + \frac{Jm}{2} + i\Gamma\right)\langle\langle d_\uparrow^\dagger|m\rangle\langle m|; d_\uparrow\rangle\rangle_\omega$$
$$= \frac{1}{2S+1} + t\langle\langle f^\dagger|m\rangle\langle m|; d_\uparrow\rangle\rangle_\omega + \Delta\langle\langle f|m\rangle\langle m|; d_\uparrow\rangle\rangle_\omega.$$
$$\text{(A2)}$$

The other two terms are given by

$$\left(\omega^+ + \varepsilon_\uparrow + \frac{Jm}{2} + i\Gamma\right)\langle\langle d_\uparrow^\dagger|m\rangle\langle m|; d_\uparrow^\dagger\rangle\rangle_\omega$$
$$= t\langle\langle f^\dagger|m\rangle\langle m|; d_\uparrow^\dagger\rangle\rangle_\omega + \Delta\langle\langle f|m\rangle\langle m|; d_\uparrow^\dagger\rangle\rangle_\omega \qquad \text{(A3)}$$

and

$$\left(\omega^+ - \varepsilon_\uparrow - \frac{Jm}{2} + i\Gamma\right)\langle\langle d_\uparrow|m\rangle\langle m|; d_\uparrow\rangle\rangle_\omega$$
$$= -t\langle\langle f|m\rangle\langle m|; d_\uparrow\rangle\rangle_\omega - \Delta\langle\langle f^\dagger|m\rangle\langle m|; d_\uparrow\rangle\rangle_\omega. \qquad \text{(A4)}$$

And, finally, the last two GFs associated with the f site is

$$\langle\langle f|m\rangle\langle m|; d_\uparrow\rangle\rangle_\omega = \frac{-t}{(\omega^+ - \varepsilon_M)}\langle\langle d_\uparrow|m\rangle\langle m|; d_\uparrow\rangle\rangle_\omega$$
$$+ \frac{\Delta}{(\omega^+ - \varepsilon_M)}\langle\langle d_\uparrow^\dagger|m\rangle\langle m|; d_\uparrow\rangle\rangle_\omega \quad \text{(A5)}$$

and

$$\langle\langle f^\dagger|m\rangle\langle m|; d_\uparrow\rangle\rangle_\omega = \frac{t}{(\omega^+ + \varepsilon_M)}\langle\langle d_\uparrow^\dagger|m\rangle\langle m|; d_\uparrow\rangle\rangle_\omega$$
$$- \frac{\Delta}{(\omega^+ + \varepsilon_M)}\langle\langle d_\uparrow|m\rangle\langle m|; d_\uparrow\rangle\rangle_\omega. \quad \text{(A6)}$$

With this group of GFs, we can determine the complete description of the QI.

APPENDIX B: QUANTUM TRANSPORT FORMALISM

Based on the quantum transport Keldysh formalism of Ref. [57], here we wrap up a summary of steps in deriving Eqs. (6), (7), and (11), which assumes the subgap regime $|eV| \ll \Delta_{SC} \to \infty$ (infinite superconducting gap standard approximation) and wide-band limit characterized by an electron-hole symmetry in the QI-leads coupling, which is given by Γ [see the main text below Eq. (1)]. As a result, we have as the total current I_α at the metallic lead α the following:

$$I_\alpha = I_\alpha^{\text{ET}} + I_\alpha^{\text{LAR}} + I_\alpha^{\text{CAR}}, \qquad \text{(B1)}$$

where

$$I_\alpha^{\text{ET}} = \frac{e}{h}\int d\varepsilon \tau_{\alpha\bar{\alpha}}^{\text{ET}}(\varepsilon)\big[f_\alpha^e(\varepsilon) - f_{\bar{\alpha}}^e(\varepsilon)\big], \qquad \text{(B2)}$$

$$I_\alpha^{\text{CAR}} = \frac{e}{h}\int d\varepsilon \tau_{\alpha\bar{\alpha}}^{\text{CAR}}(\varepsilon)\big[f_\alpha^e(\varepsilon) - f_{\bar{\alpha}}^h(\varepsilon)\big], \qquad \text{(B3)}$$

and

$$I_\alpha^{\text{LAR}} = \frac{e}{h}\int d\varepsilon \tau_{\alpha\alpha}^{\text{LAR}}(\varepsilon)\big[f_\alpha^e(\varepsilon) - f_\alpha^h(\varepsilon)\big], \qquad \text{(B4)}$$

where I_α^{ET} and I_α^{CAR} refer to the currents for the ET and crossed Andreev reflection (CAR) between the QI and the lead α, but with occupation probabilities of an electron $f_{\bar{\alpha}}^e(\varepsilon)$ and hole $f_{\bar{\alpha}}^h(\varepsilon)$ states at lead $\bar{\alpha}$, respectively, where $f_\alpha^j(\varepsilon)$ stands for the Fermi distribution at lead α and $j = e(h)$ for the electron (hole) quasiparticle. For I_α^{LAR}, the hole emission is in the same terminal α, once it depends on $f_\alpha^h(\varepsilon)$.

As the total current should conserve, Kirchhoff's law holds $I_\alpha + I_{\bar{\alpha}} + I_S = 0$. Additionally, the following assumptions are performed: $\mu_{\text{source}} = -\mu_{\text{drain}} = eV/2$ and the TSC is supposed to be grounded (null chemical potential $\mu_{\text{SC}} = 0$). The former implies $f_\alpha^e(\varepsilon) = f_{\bar{\alpha}}^h(\varepsilon)$ and, consequently, $I_\alpha^{\text{CAR}} = 0$ from Eq. (B3), while the latter gives $I_S = 0$ and finally $I_\alpha = -I_{\bar{\alpha}}$. It means that the current only changes signs from terminal α to $\bar{\alpha}$, the conductance $\mathcal{G}_{\text{total}}$ being lead independent:

$$\mathcal{G}_{\text{total}} = \frac{dI_\alpha}{dV} = \frac{dI_\alpha^{\text{ET}}}{dV} + \frac{dI_\alpha^{\text{LAR}}}{dV} = \mathcal{G}_{\text{ET}} + \mathcal{G}_{\text{LAR}}, \qquad \text{(B5)}$$

with

$$\frac{dI_\alpha^{\text{ET}}}{dV} = \frac{e^2}{2h}\frac{1}{T}\int d\varepsilon \tau_{\alpha\bar{\alpha}'}^{\text{ET}}(\varepsilon)\big\{f_\alpha^e(\varepsilon)\big[1 - f_\alpha^e(\varepsilon)\big]$$
$$+ f_{\bar{\alpha}}^e(\varepsilon)\big[1 - f_{\bar{\alpha}}^e(\varepsilon)\big]\big\} \qquad \text{(B6)}$$

and

$$\frac{dI_\alpha^{\text{LAR}}}{dV} = \frac{e^2}{2h}\frac{1}{T}\int d\varepsilon \tau_{\alpha\alpha}^{\text{LAR}}(\varepsilon)\big\{f_\alpha^e(\varepsilon)\big[1 - f_\alpha^e(\varepsilon)\big]$$
$$+ f_{\bar{\alpha}}^e(\varepsilon)\big[1 - f_{\bar{\alpha}}^e(\varepsilon)\big]\big\}, \qquad \text{(B7)}$$

where we employed the identity $f_\alpha^e(\varepsilon) = f_{\bar{\alpha}}^h(\varepsilon)$ again and

$$\frac{\partial f_{\alpha(\bar{\alpha})}^e(\varepsilon)}{\partial V} = \pm\frac{e}{2T}f_{\alpha(\bar{\alpha})}^e(\varepsilon)\big[1 - f_{\alpha(\bar{\alpha})}^e(\varepsilon)\big], \qquad \text{(B8)}$$

with $k_B = 1$, $f_\alpha^e(\varepsilon) = f(\varepsilon - eV/2)$, $f_{\bar{\alpha}}^e(\varepsilon) = f(\varepsilon + eV/2)$, and $f(x) = 1/(1 + e^{x/T})$.

As $\frac{1}{T}f_{\alpha(\bar{\alpha})}^e(\varepsilon)[1 - f_{\alpha(\bar{\alpha})}^e(\varepsilon)]) = (-\frac{\partial f_{\alpha(\bar{\alpha})}^e(\varepsilon)}{\partial\varepsilon}) \to \delta(\varepsilon \mp eV/2)$ when $T \to 0$ K, then we deduce Eqs. (6) and (7). To conclude, we should remember that the Keldysh formalism of Ref. [57] also ensures

$$I_\alpha = \frac{e}{h}\int d\varepsilon(-\Gamma\text{Im}\langle\langle d_\uparrow; d_\uparrow^\dagger\rangle\rangle_\omega)\big[f_\alpha^e(\varepsilon) - f_{\bar{\alpha}}^e(\varepsilon)\big]. \qquad \text{(B9)}$$

Therefore, by comparing Eqs. (B9) and (B1), together with Eqs. (B2) and (B4), we finally determine Eq. (11).

APPENDIX C: GREEN'S FUNCTIONS FOR THE SYSTEM RIGHT SIDE

Here we show the GFs for the f orbital site and the MZMs γ_1 and γ_2 of the Kitaev dimer's right side [Eq. (3)]. These quantities are important for Fig. 5 and make explicit the poor man's Majorana [55,56] and ABS [33] regimes in our system. As we know that $\gamma_1 = \frac{1}{\sqrt{2}}(f^\dagger + f)$ and $\gamma_2 = \frac{i}{\sqrt{2}}(f^\dagger - f)$, we naturally find the GF

$$\langle\langle \gamma_j; \gamma_j \rangle\rangle_\omega = \tfrac{1}{2}[\langle\langle f; f^\dagger \rangle\rangle_\omega + \langle\langle f^\dagger; f \rangle\rangle_\omega$$
$$+ \epsilon(\langle\langle f^\dagger; f^\dagger \rangle\rangle_\omega + \langle\langle f; f \rangle\rangle_\omega)], \quad \text{(C1)}$$

where $j = (1, 2)$ corresponds to $\epsilon = (+1, -1)$, respectively. By applying Eq. (10) for the EOM approach, we obtain

$$\langle\langle f; f^\dagger \rangle\rangle_\omega = \frac{1}{(2S+1)} \sum_m \frac{1}{(\omega^+ - \varepsilon_M - \Sigma_{+M})}, \quad \text{(C2)}$$

$$\langle\langle f^\dagger; f \rangle\rangle_\omega = \frac{1}{(2S+1)} \sum_m \frac{1}{(\omega^+ + \varepsilon_M - \Sigma_{-M})}, \quad \text{(C3)}$$

$$\langle\langle f^\dagger; f^\dagger \rangle\rangle_\omega = \frac{1}{(2S+1)} \sum_m \frac{2\Delta t K_{-M}}{(\omega^+ + \varepsilon_M - \Sigma_{-M})}, \quad \text{(C4)}$$

and

$$\langle\langle f; f \rangle\rangle_\omega = \frac{1}{(2S+1)} \sum_m \frac{2\Delta t K_{+M}}{(\omega^+ - \varepsilon_M - \Sigma_{+M})}, \quad \text{(C5)}$$

with $\Sigma_{\pm M} = K_C^\pm + (2\Delta t)^2 K_D K_{\pm M}$ being the self-energy due to the interaction of the f site with the QI, which can be expressed in terms of the defined quantities

$$K_{+M} = \frac{K_D}{(\omega^+ + \varepsilon_M - K_C^-)}, \quad \text{(C6)}$$

$$K_{-M} = \frac{K_D}{(\omega^+ - \varepsilon_M - K_C^+)}, \quad \text{(C7)}$$

$$K_D = \frac{(\omega + i\eta^+) + i\Gamma}{(\omega + i\Gamma + i\eta^+)^2 - \varepsilon_\uparrow^2 - Jm[\varepsilon_\uparrow + \frac{Jm}{4}]}, \quad \text{(C8)}$$

and

$$K_C^\pm = \left[\frac{(\omega + i\eta^+)(t^2 + \Delta^2) \pm \varepsilon_\uparrow(t^2 - \Delta^2)}{(\omega + i\Gamma + i\eta^+)^2 - \varepsilon_\uparrow^2 - Jm[\varepsilon_\uparrow + \frac{Jm}{4}]} \right]$$
$$+ \left[\frac{\pm\frac{Jm}{2}(t^2 - \Delta^2) + i\Gamma(t^2 + \Delta^2)}{(\omega + i\Gamma + i\eta^+)^2 - \varepsilon_\uparrow^2 - Jm[\varepsilon_\uparrow + \frac{Jm}{4}]} \right]. \quad \text{(C9)}$$

[1] E. Majorana, Nuovo Cim. **14**, 171 (1937).
[2] P. Marra, J. Appl. Phys. **132**, 231101 (2022).
[3] D. E. Liu and H. U. Baranger, Phys. Rev. B **84**, 201308(R) (2011).
[4] E. Vernek, P. H. Penteado, A. C. Seridonio, and J. C. Egues, Phys. Rev. B **89**, 165314 (2014).
[5] M. Duckheim and P. W. Brouwer, Phys. Rev. B **83**, 054513 (2011).
[6] R. M. Lutchyn, J. D. Sau, and S. Das Sarma, Phys. Rev. Lett. **105**, 077001 (2010).
[7] O. Lesser and Y. Oreg, J. Phys. D **55**, 164001 (2022).
[8] F. Pientka, L. I. Glazman, and F. von Oppen, Phys. Rev. B **89**, 180505(R) (2014).
[9] Y. Oreg, G. Refael, and F. von Oppen, Phys. Rev. Lett. **105**, 177002 (2010).
[10] F. Pientka, L. I. Glazman, and F. von Oppen, Phys. Rev. B **88**, 155420 (2013).
[11] J. Li, H. Chen, I. K. Drozdov, A. Yazdani, B. A. Bernevig, and A. H. MacDonald, Phys. Rev. B **90**, 235433 (2014).
[12] J. Klinovaja, P. Stano, A. Yazdani, and D. Loss, Phys. Rev. Lett. **111**, 186805 (2013).
[13] S. Nadj-Perge, I. K. Drozdov, B. A. Bernevig, and A. Yazdani, Phys. Rev. B **88**, 020407(R) (2013).
[14] L. Fu and C. L. Kane, Phys. Rev. B **79**, 161408(R) (2009).
[15] L. Fu and C. L. Kane, Phys. Rev. Lett. **100**, 096407 (2008).
[16] M. M. Vazifeh and M. Franz, Phys. Rev. Lett. **111**, 206802 (2013).
[17] S. Nakosai, Y. Tanaka, and N. Nagaosa, Phys. Rev. B **88**, 180503(R) (2013).
[18] B. Braunecker and P. Simon, Phys. Rev. Lett. **111**, 147202 (2013).
[19] A. C. Potter and P. A. Lee, Phys. Rev. B **85**, 094516 (2012).

[20] S. B. Chung, H.-J. Zhang, X.-L. Qi, and S.-C. Zhang, Phys. Rev. B **84**, 060510(R) (2011).
[21] C. W. J. Beenakker, Rev. Mod. Phys. **87**, 1037 (2015).
[22] M. Sato and S. Fujimoto, J. Phys. Soc. Jpn. **85**, 072001 (2016).
[23] M. Sato and Y. Ando, Rep. Prog. Phys. **80**, 076501 (2017).
[24] A. Haim and Y. Oreg, Phys. Rep. **825**, 1 (2019).
[25] J. Alicea, Rep. Prog. Phys. **75**, 076501 (2012).
[26] C. Beenakker, Annu. Rev. Condens. Matter Phys. **4**, 113 (2013).
[27] K. Flensberg, F. von Oppen, and A. Stern, Nat. Rev. Mater. **6**, 944 (2021).
[28] K. Laubscher and J. Klinovaja, J. Appl. Phys. **130**, 081101 (2021).
[29] M. T. Deng, S. Vaitiekenas, E. B. Hansen, J. Danon, M. Leijnse, K. Flensberg, J. Nygard, P. Krogstrup, and C. M. Marcus, Science **354**, 1557 (2016).
[30] V. Mourik, K. Zuo, S. M. Frolov, S. R. Plissard, E. P. A. M. Bakkers, and L. P. Kouwenhoven, Science **336**, 1003 (2012).
[31] F. Nichele, A. C. C. Drachmann, A. M. Whiticar, E. C. T. O'Farrell, H. J. Suominen, A. Fornieri, T. Wang, G. C. Gardner, C. Thomas, A. T. Hatke, P. Krogstrup, M. J. Manfra, K. Flensberg, and C. M. Marcus, Phys. Rev. Lett. **119**, 136803 (2017).
[32] A. Y. Kitaev, Phys. Usp. **44**, 131 (2001).
[33] M.-T. Deng, S. Vaitiekėnas, E. Prada, P. San-Jose, J. Nygård, P. Krogstrup, R. Aguado, and C. M. Marcus, Phys. Rev. B **98**, 085125 (2018).
[34] L. S. Ricco, M. de Souza, M. S. Figueira, I. A. Shelykh, and A. C. Seridonio, Phys. Rev. B **99**, 155159 (2019).
[35] C.-X. Liu, J. D. Sau, T. D. Stanescu, and S. Das Sarma, Phys. Rev. B **96**, 075161 (2017).

[36] L. S. Ricco, J. E. Sanches, Y. Marques, M. de Souza, M. S. Figueira, I. A. Shelykh, and A. C. Seridonio, Sci. Rep. **11**, 17310 (2021).

[37] S. Nadj-Perge, I. K. Drozdov, J. Li, H. Chen, S. Jeon, J. Seo, A. H. MacDonald, B. A. Bernevig, and A. Yazdani, Science **346**, 602 (2014).

[38] M. Ruby, F. Pientka, Y. Peng, F. von Oppen, B. W. Heinrich, and K. J. Franke, Phys. Rev. Lett. **115**, 197204 (2015).

[39] R. Pawlak, M. Kisiel, J. Klinovaja, T. Meier, S. Kawai, T. Glatzel, D. Loss, and E. Meyer, npj Quantum Inf. **2**, 16035 (2016).

[40] S. R. Elliott and M. Franz, Rev. Mod. Phys. **87**, 137 (2015).

[41] R. Aguado, Riv. Nuovo Cimento **40**, 523 (2017).

[42] M. Leijnse and K. Flensberg, Semicond. Sci. Technol. **27**, 124003 (2012).

[43] T. D. Stanescu and S. Tewari, J. Phys.: Condens. Matter **25**, 233201 (2013).

[44] T.-P. Choy, J. M. Edge, A. R. Akhmerov, and C. W. J. Beenakker, Phys. Rev. B **84**, 195442 (2011).

[45] S. Jeon, Y. Xie, J. Li, Z. Wang, B. A. Bernevig, and A. Yazdani, Science **358**, 772 (2017).

[46] P. Marra and M. Nitta, Phys. Rev. B **100**, 220502(R) (2019).

[47] R. Pawlak, S. Hoffman, J. Klinovaja, D. Loss, and E. Meyer, Prog. Part. Nucl. Phys. **107**, 1 (2019).

[48] B. Jäck, Y. Xie, and A. Yazdani, Nat. Rev. Phys. **3**, 541 (2021).

[49] G. Górski, J. Baranski, I. Weymann, and T. Domanski, Sci. Rep. **8**, 15717 (2018).

[50] C. Nayak, S. H. Simon, A. Stern, M. Freedman, and S. Das Sarma, Rev. Mod. Phys. **80**, 1083 (2008).

[51] S. D. Sarma, M. Freedman, and C. Nayak, npj Quantum Inf. **1**, 15001 (2015).

[52] R. Wiesendanger, Rev. Mod. Phys. **81**, 1495 (2009).

[53] P. W. Anderson, Phys. Rev. **124**, 41 (1961).

[54] E. Prada, R. Aguado, and P. San-Jose, Phys. Rev. B **96**, 085418 (2017).

[55] M. Leijnse and K. Flensberg, Phys. Rev. B **86**, 134528 (2012).

[56] T. Dvir, G. Wang, N. van Loo, C.-X. Liu, G. P. Mazur, A. Bordin, S. L. D. ten Haaf, S. L. D. ten Haaf, J.-Y. Wang, D. van Driel, F. Zatelli, X. Li, F. K. Malinowski, S. Gazibegovic, G. Badawy, E. P. A. M. Bakkers, M. Wimmer, and L. P. Kouwenhoven, Nature (London) **614**, 445 (2023).

[57] L. Máthé, D. Sticlet, and L. P. Zârbo, Phys. Rev. B **105**, 155409 (2022).

[58] D. N. Zubarev, Sov. Phys. Usp. **3**, 320 (1960).

[59] H. Bruus and K. Flensberg, *Many-Body Quantum Theory in Condensed Matter Physics, An Introduction* (Oxford University Press, Oxford, 2012).